

Article

A Facile Synthesis of ZrO_x - $MnCO_3$ /Graphene Oxide (GRO) Nanocomposites for the Oxidation of Alcohols using Molecular Oxygen under Base Free Conditions

Syed Farooq Adil ^{1,*}, Mohamed E. Assal ¹, Mohammed Rafi Shaik ¹, Mufsir Kuniyil ², Nawaf M. AlOtaibi ¹, Mujeeb Khan ¹, Muhammad Sharif ³, M. Mujahid Alam ⁴, Abdulrahman Al-Warthan ¹, Jabair Ali Mohammed ⁵, Mohammed Rafiq H Siddiqui ^{1,*} and Muhammad Nawaz Tahir ^{3,*}

¹ Department of Chemistry, College of Science, King Saud University, P.O. 2455, Riyadh 11451, Saudi Arabia

² Department of Chemistry, Koneru Lakshmaiah Education Foundation, Vaddeswaram, Guntur 522502, India

³ Chemistry Department, King Fahd University of Petroleum and Materials, Dhahran 31261, Saudi Arabia

⁴ Department of Chemistry, College of Science, King Khalid University, Abha 62529, Saudi Arabia

⁵ Center of Excellence for Research in Engineering Materials (CEREM), King Saud University, P. O. Box 800, Al-Riyadh 11421, Saudi Arabia

* Correspondence: sfadil@ksu.edu.sa (S.F.A.); rafiqs@ksu.edu.sa (M.R.H.S.); muhammad.tahir@kfupm.edu.sa (M.N.T.)

Received: 9 June 2019; Accepted: 28 August 2019; Published: 10 September 2019



Abstract: Graphene and its nanocomposites are showing excellent potential in improving the catalytic performances of different materials. However, the synthetic protocol and its form, such as graphene oxide (GRO) or highly reduced graphene oxide (HRG), influence the catalytic efficiencies. Here, we present, a facile synthesis of graphene oxide (GRO) and ZrO_x - $MnCO_3$ -based nanocomposites [(1%) ZrO_x - $MnCO_3$ /(x%)GRO] and their outcome as an oxidation catalyst for alcohol oxidation under mild conditions using O_2 as a clean oxidant. The ZrO_x - $MnCO_3$ /GRO catalyst prepared by incorporating GRO to pre-calcined ZrO_x - $MnCO_3$ using ball milling showed remarkable enhancement in the catalytic activities as compared to pristine ZrO_x - $MnCO_3$, ZrO_x - $MnCO_3$ supported on HRG or ZrO_x - $MnCO_3$ /GRO prepared by in-situ growth of ZrO_x - $MnCO_3$ onto GRO followed by calcination. The catalyst with composition (1%) ZrO_x - $MnCO_3$ /(1%)GRO exhibited superior specific activity (57.1 mmol/g·h) with complete conversion and >99% selectivity of the product within a short period of time (7 min) and at a relatively lower temperature (100 °C). The catalyst could be recycled at least five times with a negligible decrease in efficiency and selectivity. The catalytic study was extended to different aromatic as well as aliphatic alcohols under optimized conditions, which confirmed the efficiency and selectivity of the catalyst.

Keywords: heterogeneous catalysis; ZrO_x - $MnCO_3$ /GRO-based nanocomposites; oxidation of alcohols

1. Introduction

Catalytic oxidation of alcohols into respective aldehydes and ketones is a pivotal reaction in organic syntheses, because it produces valued precursors in agrochemicals, food processing, confectionary, fragrances, dyestuffs, insecticides, flame-retardants, and pharmaceuticals industries [1,2]. Conventionally, alcohol oxidation has relied on the utilization of toxic and corrosive stoichiometric inorganic oxidants, like chromium oxides, hypochlorite, Dess-Martin periodinane, or permanganate. These are usually costly oxidants and suffer from the generation of significant amounts of hazardous wastes, such as CrO_3 , $Na_2Cr_2O_7$, SeO_2 , RuO_4 , $NaClO$, $KMnO_4$, and PCC [3,4]. In order to reduce the toxic waste, selective alcohol oxidation reactions are carried out using molecular O_2 as a terminal

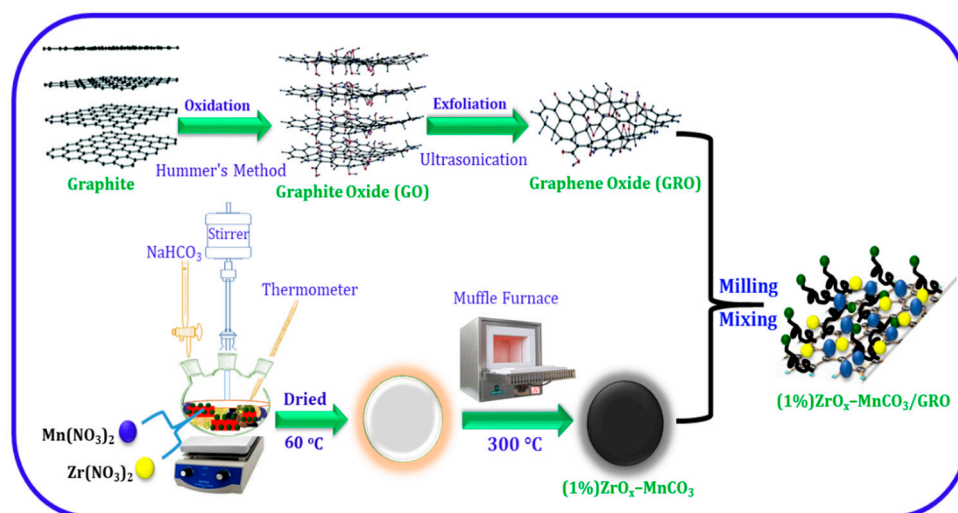
oxidizing agent. This has emerged as an environment-friendly method, because oxygen is natural, readily accessible, inexpensive, and produces water as a sole by-product. Consequently, massive efforts have been devoted to the enhancement of catalytic oxidation methods [5]. In this regard, noble metals, e.g., Au [6], Pt [7], Pd [8], and Ru [9], were widely utilized as a heterogeneous catalyst for this chemical transformation and exhibit high catalytic activities. However, these precious metals suffer from some disadvantages, such as low abundance, toxicity, and high cost [10]. Hence, huge efforts have been devoted to the substitution of these noble metals with cost-effective and abundant transitional metals, such as Co [11], Fe [12], Cu [13], Mo [14], V [15], and Zn [16], for catalytic oxidation of alcohols.

Transition metals or metal oxide are found to be highly efficacious catalysts for the oxidation of alcohol. Furthermore, the catalytic efficiency of these catalysts can be enhanced by improving the structural architecture (nanocomposites) that in turn helps to increase the surface area [17]. Surface area can also be increased by synthesizing the materials in a nano-sized regime, but small-sized nanoparticles are not stable and easily aggregate due to high surface energy, which normally decreases their performances and stabilities [18].

This problem can be solved by immobilizing nano-sized materials on a suitable support that offers high surface area and prevents nanoparticles from agglomeration [19]. Among the various supports tested, carbon-based materials, especially graphene and its derivatives, such as HRG and GRO, have received enormous interest because of their tremendous potential in different applications, including electronics, solar cells, sensors, catalysis, batteries, water purification, and drug delivery. This is attributed to the extraordinary chemical, electronic, and physical properties related to their structural integrity and high surface area [20,21]. Inspired by these excellent properties, we previously used HRG as a support for various nanostructured oxidation catalysts. However, the immobilization of catalyst is always a challenge onto a reduced support. In contrast, GRO is known to be an exemplary supporting material owing to its inherited oxygen functionalities introduced during its synthesis. As an example, the oxidation process (Hummer's procedure) GRO's surface has myriad oxygenic-carrying groups, including hydroxyl, epoxy, carbonyl, and carboxyl groups, which provide a perfect platform to bind metal oxides nanomaterials [22]. Moreover, these functional groups are responsible for its moderate acidic and oxidizing properties [23].

Various metal or metal oxide NPs, such as Au [24], Pd [25], Fe₂O₃ [26], Co₃O₄ [27], and ZnO [28], have been immobilized onto GRO nanosheets, which exhibited outstanding catalytic activity and selectivity. In particular, graphene oxide-based metal or metal oxide nanocomposites are utilized as an efficacious oxidation catalyst for the oxidation of numerous organic moieties, such as alcohols [19,29], cyclohexane [30,31], amines [32], olefins [33], benzene [34], and ethylbenzene [35]. In all these catalysts, the GRO support was found to play a key role in the effectiveness as a catalyst both from the architecture to the functional level.

In this contribution, we report on a facile preparation of GRO–ZrO_x–MnCO₃ NPs-based nanocomposites synthesized by mixing GRO with pre-calcined ZrO_x–MnCO₃ using ball milling. The ball milling helps to reduce the size of nanoparticles and prevents agglomeration. The as-synthesized catalysts are tested for the selective oxidation of a various kinds of alcohols to comprehend the effect of graphene oxide in the catalyst system (Scheme 1). To the best of our knowledge, this is the first study using ZrO_x-doped MnCO₃-supported GRO as catalyst for the oxidation of alcohols and particularly, highlighting the role of GRO as a support material. At the end, we will also present a short comparison of the role of GRO or HRG as a support material (with reference to our previous experience).



Scheme 1. Synthetic illustration of the synthesis of (1%)ZrO_x-MnCO₃/GRO nanocomposite.

2. Results

2.1. Characterizations

The crystallinity of the prepared materials was monitored using X-ray diffraction (XRD). To compare, the XRD patterns of pure graphite, GRO, (1%)ZrO_x-MnCO₃, and (1%)ZrO_x-MnCO₃/(1%)GRO are displayed in Figure 1. Pristine graphite exhibits a sharp peak at 2θ of 26.5° , which is ascribed to the (0 0 2) crystal plane of stacked carbon layers with a *d*-spacing of 3.41 Å [36]. In case of GRO, a wide distinct reflection at 2θ (11.8°) is a characteristic reflection of GRO. The disappearance of the reflection at 2θ of 26.5° confirms effective oxidation of graphite to GRO using the Hummer method [37]. This shift led to an increase in the *d*-spacing from 3.41 to 4.85 Å for graphite and GRO, attributed to the inclusion of various O-carrying groups on the surface [38]. The XRD pattern of (1%)ZrO_x-MnCO₃ without graphene support matches well with the certified data of rhodochrosite manganese carbonate (JCPDS No. 1-0981) in addition to the peaks marked with stars due to the presence of ZrO_x [39]. In the case of (1%)ZrO_x-MnCO₃/(1%)GRO nanocomposite, the reflection at 2θ of 11.8° , in addition to the reflections of rhodochrosite manganese carbonate, confirms the formation of nanocomposites.

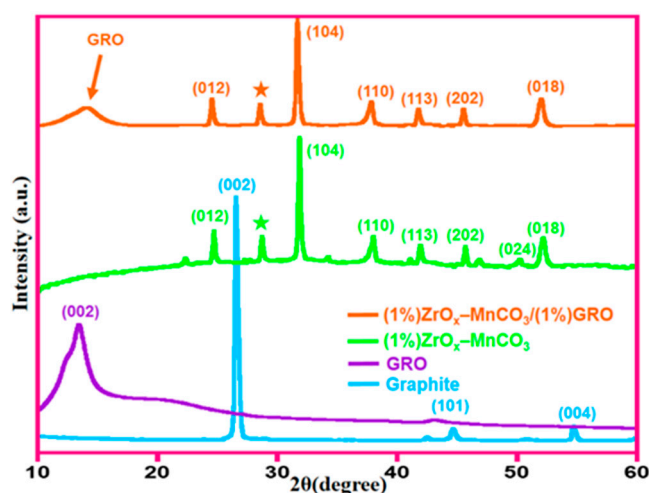


Figure 1. XRD patterns of graphite, GRO, (1%)ZrO_x-MnCO₃, and (1%)ZrO_x-MnCO₃/(1%)GRO.

Thermal gravimetric analysis (TGA) was performed to identify the thermal stability of the (1%)ZrO_x-MnCO₃/(1%)GRO nanocomposite and was compared to the thermal behavior of the precursors, like pure graphite, GRO, and un-supported catalyst (1%)ZrO_x-MnCO₃, as displayed in Figure 2. Samples were heated from room temperature (RT) to 800 °C with a heating rate of 10 °C/min under an inert atmosphere. The TGA results apparently illustrated that the thermal stability of GRO is much lower than graphite owing to the presence of O-carrying functional groups on the GRO surface. The TGA thermogram of graphite exhibited a weight loss of approximately 1% [40]. On the contrary, GRO was found to be thermally unstable, wherein at 100 °C, it starts to lose absorbed moisture and volatile impurities. Approximately 43% of the weight was lost in the range of 200 to 370 °C, which could be due to pyrolysis of the oxygenated groups [41]. In comparison, the (1%)ZrO_x-MnCO₃ on the GRO support showed a much improved thermal stability. The overall weight loss, i.e., 11%, in the range of 370 to 800 °C [42] could be attributed to the thermal degradation of GRO upon exposure to an increase of temperature. This data is consistent with an earlier reported study [43].

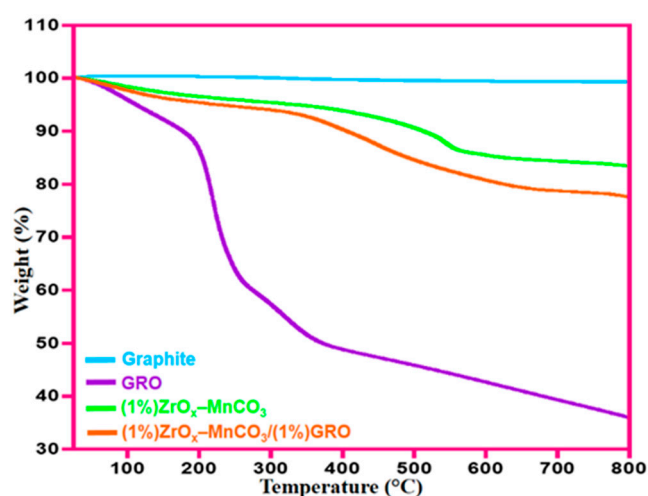


Figure 2. TGA curves of the graphite, GRO, (1%)ZrO_x-MnCO₃, and (1%)ZrO_x-MnCO₃/(1%)GRO.

Raman spectroscopy is the most significant tool for the structural investigation of carbonaceous materials. Figure 3 illustrates the Raman spectra of (1%)ZrO_x-MnCO₃ and (1%)ZrO_x-MnCO₃/(1%)GRO samples. The Raman spectra of (1%)ZrO_x-MnCO₃ and (1%)ZrO_x-MnCO₃/(1%)GRO nanocomposite exhibited two characteristic peaks of manganese carbonate located at 725 and 1080 cm⁻¹, indicating that the existence of Mn as MnCO₃ in both (1%)ZrO_x-MnCO₃ as well as (1%)ZrO_x-MnCO₃/(1%)GRO nanocomposites [44]. For GRO, the D-band is related to the defects or disorder in the graphite structure and the G-band is associated to the well-ordered structure of the vibrations of the *sp*²-hybridized carbon framework [45]. In the case of (1%)ZrO_x-MnCO₃/(1%)GRO, the G- and the D-bands are situated at 1604 and 1347 cm⁻¹, respectively. The relative ratio of these bands shows the demolition of the *sp*² structure by the oxidation process and the existence of oxygenic functionalities [46].

Figure 4 depicts the FT-IR spectra of GRO and the (1%)ZrO_x-MnCO₃/(1%)GRO nanocomposite. In the case of GRO, a broad-ranging band at approximately 3440 cm⁻¹ is due to stretching vibration mode of hydroxyl (O-H) groups due to the presence of oxygen-containing functional groups. The characteristic absorption peak belonging to carbonyl groups' (C=O) stretching of (-COOH) groups was observed at 1738 cm⁻¹ and the absorption peak located at 1630 cm⁻¹ corresponding to the stretching vibration of the carbon backbone (C=C/C-C) from the graphitic domains [47]. The three absorption peaks approximately situated at 1398, 1226, and 1060 cm⁻¹ are attributed to the vibration modes of (C-OH), (C-O-C), and (C-O), respectively [48]. The spectrum of (1%)ZrO_x-MnCO₃/(1%)GRO displayed the characteristic absorption peaks of most of oxygenated groups (1738 cm⁻¹ (C=O) and 1060 cm⁻¹ (C-O)) with a strong band at 1380 cm⁻¹, related to the carbonate groups and the sharp strong peak located nearly at 585 cm⁻¹ corresponds to vibrations of different Mn-O bonds [49].

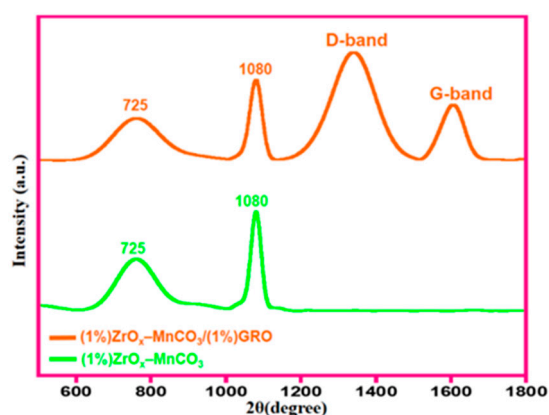


Figure 3. Raman spectra of un-supported (1%)ZrO_x-MnCO₃ catalyst and (1%)ZrO_x-MnCO₃/(1%)GRO nanocomposite.

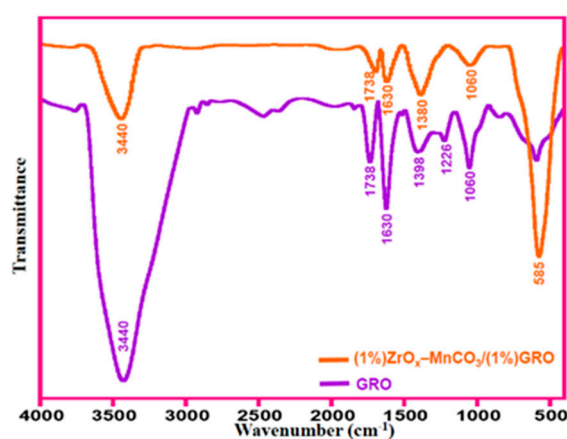


Figure 4. FT-IR spectra of GRO and (1%)ZrO_x-MnCO₃/(1%)GRO nanocomposite.

The morphology of the as-synthesized (1%)ZrO_x-MnCO₃ and (1%)ZrO_x-MnCO₃/(1%)GRO catalyst after ball milling to prepare a homogeneous catalyst was studied using SEM (Figure 5). The SEM micrographs of (1%)ZrO_x-MnCO₃ catalyst exhibited well-defined cuboidal-shaped microparticles (Figure 5a). However, the (1%)ZrO_x-MnCO₃/(1%)GRO nanocomposites (Figure 5b) also exhibited cuboidal-shaped particles with a majority of rather small-sized crystals due to ball milling. The corresponding histograms depicting the particles' size and size distribution (before and after ball milling) are given as Supplementary Material (Figure S1). The nanoparticles after ball milling resulted in a smaller but broad size distribution. This increases the overall surface area of the catalyst. The elemental analysis of the as-fabricated (1%)ZrO_x-MnCO₃/(1%)GRO nanocomposite using EDX (Figure 6) showed the presence of Zr, Mn, O, and C in an appropriate ratio, close to the stoichiometric values as distinctly displayed in the EDX spectrum.

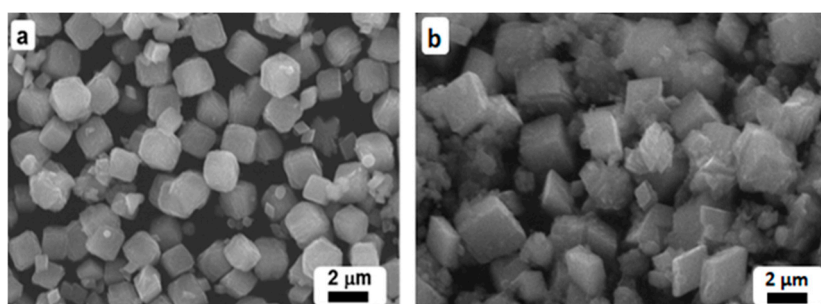


Figure 5. SEM micrographs of (a) (1%)ZrO_x-MnCO₃ and (b) (1%)ZrO_x-MnCO₃/(1%)GRO.

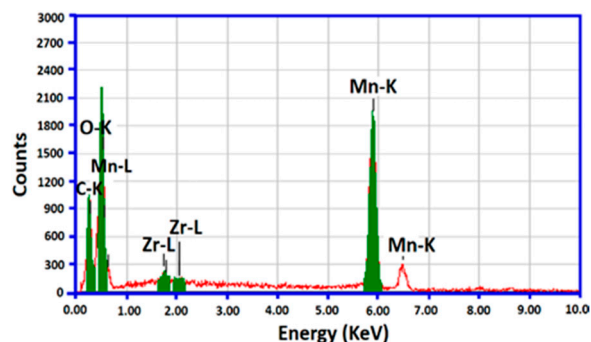
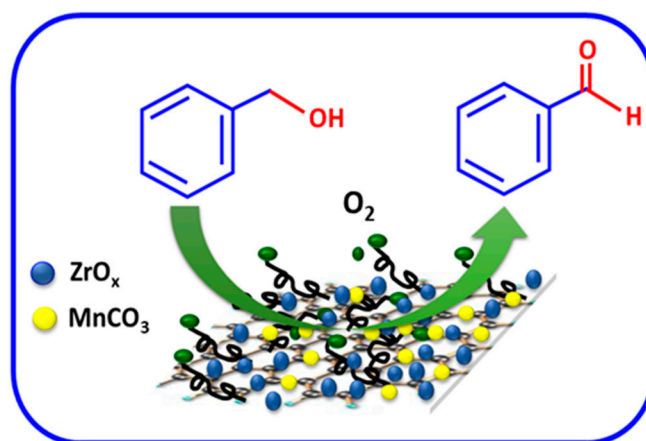


Figure 6. Energy dispersive X-ray spectroscopy (EDX) indicating the chemical composition of the (1%)ZrO_x-MnCO₃/(1%)GRO nanocomposite.

To identify the specific surface area of the as-obtained catalysts and explore its relationship with the efficacy of the catalytic protocol for the oxidation of benzyl alcohol (BzOH), the samples were analyzed using Brunauer–Emmett–Teller (BET) analysis. The specific surface area of the (1%)ZrO_x-MnCO₃ without GRO is about 134 m²/g as illustrated in Table 1. Whilst the surface areas of the nanocomposites after incorporating the catalyst with (1%)GRO significantly increased to 230 m²/g. This agrees well with the SEM results, which showed the presence of small-sized (1%)ZrO_x-MnCO₃ particles covering the surface. It is worth mentioning that the catalytic results are very much in accordance with the surface area as per the BET data. Therefore, it can be concluded that both the graphene and synthetic method have a positive impact on increasing the surface area of the synthesized catalysts, which in turn increases the catalytic efficiency of the as-fabricated nanocomposites.

2.2. Catalytic Studies

The oxidation of BzOH using molecular oxygen (O₂) was chosen as the probe reaction as demonstrated in Scheme 2 and the reaction circumstances were optimized in detail as demonstrated in Table 1 and Figures 7–10.



Scheme 2. Schematic representation of BzOH oxidation using O₂ catalyzed by the as-obtained nanocomposite.

2.2.1. Impact of GRO on the Catalytic Activity

The catalytic efficiency of the oxidation catalyst can be fine-tuned using graphene as the support and an effective promoter [29,50,51]. In our former publication, we found that zirconia was found to be a perfect promoter for manganese carbonate, and the (1%)ZrO_x-MnCO₃ catalyst calcined at 300 °C showed a superior catalytic performance towards selective oxidation of alcohols using O₂ as a clean oxidant, in which 300 mg of (1%)ZrO_x-MnCO₃ gave a complete conversion of BzOH within 30 min at

100 °C [39]. Therefore, for present work, the catalyst (1%)ZrO_x-MnCO₃ was chosen with an aim of comparing the support effects. However, it is worth mentioning that initial studies were devoted to find out the suitable weight percentage of GRO (w/w %) in the catalytic system in order to improve the catalytic performance.

Table 1. Catalytic performances of various catalysts with different percentages of GRO for BzOH oxidation.

Entry	Catalyst	Conversion (%)	Specific activity (mmol·g ⁻¹ ·h ⁻¹)	Selectivity (%)
1	GRO	2.9	1.7	>99
2	(1%)ZrO _x -MnCO ₃	74.4	42.5	>99
3	(1%)ZrO _x -MnCO ₃ /(1%)GRO	100.0	57.1	>99
4	(1%)ZrO _x -MnCO ₃ /(3%)GRO	96.1	55.0	>99
5	(1%)ZrO _x -MnCO ₃ /(5%)GRO	84.7	48.4	>99
6	(1%)ZrO _x -MnCO ₃ /(7%)GRO	68.1	38.9	>99

Conditions: 2 mmol of BzOH, 10 mL toluene, 0.3 g catalyst, 20 mL/min O₂ flow rate, 100 °C, 7 min.

Primarily, we examined the catalytic activity of pure GRO for the selective oxidation of BzOH utilizing O₂ as a clean oxidant at 100 °C. It was observed that GRO is not an effective catalyst for the BzOH oxidation (Table 1, entry 1). However, when the different percentages of GRO were incorporated into the catalytic system, i.e., (1%)ZrO_x-MnCO₃/(X%)GRO nanocomposites (where: X = 1, 3, 5, and 7), it was found to have a considerable impact on the catalytic efficiency. The best catalytic efficacy was obtained with 1% GRO inclusion. The attained results are compiled in Table 1 and presented in Figure 7.

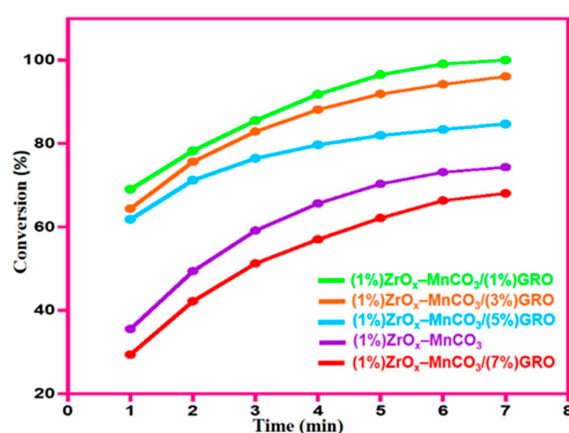


Figure 7. Graphical illustration of BzOH oxidation catalyzed by various catalysts with different percentages of GRO.

According to Table 1, it was observed that the catalyst, i.e., (1%)ZrO_x-MnCO₃, gave a 74.4% conversion of BzOH within 7 min (Table 2, entry 2). Nevertheless, after further modifications, the doping of the catalytic system with (1%) GRO, i.e., (1%)ZrO_x-MnCO₃/(1%)GRO nanocomposite, was found to be the optimum catalyst among all other catalysts with various percentages of GRO. The (1%)ZrO_x-MnCO₃/(1%)GRO nanocomposite yielded a 100% BzOH conversion after an extremely short period of just 7 min as well as superior specific activity of 57.1 mmol/g·h (Table 1, entry 3). Furthermore, it was observed that upon increasing the amount of GRO to 3%, a slight reduction in the conversion of BzOH to 96.1% was found (Table 1, entry 4). Further increasing the GRO to 5% and 7% in the catalyst system yielded a further reduction in the conversion product to 84.7% and 68.1%, respectively, under similar circumstances (Table 1, entries 5 and 6). The decrease in catalytic efficiency on increasing the GRO could be possibly ascribed to wrapping of the catalyst surface, which results

in blocking the active sites of the catalyst. Meanwhile, the selectivity towards benzaldehyde (BzH) was almost constant throughout oxidation processes (>99%) (Table 1, entries 1–6). Hence, it can be stated that the GRO plays a fundamental role in improving the effectiveness of this transformation. Furthermore, in order to ascertain that the change in catalytic efficiency was mainly due to the inclusion of GRO and not just due to the milling procedure that was carried out for the preparation of the nanocomposite, a reaction was carried out using the catalyst without GRO, i.e., (1%)ZrO_x-MnCO₃, which was subjected to the same ball milling procedure and from the results obtained it was confirmed that the milling procedure contributes slightly (2%) to the enhancement of catalytic performance. However, the inclusion of GRO induces a significant difference in the catalytic performance. The graphical representation of the results obtained is given in Figure S2.

2.2.2. Impact of Different Graphene Supports

Based on our previous study, we also compared the performance of ZrO_x NPs/MnCO₃ deposited on different graphene supports (i.e., GRO and HRG) for BzOH oxidation in order to comprehend the function of the graphene support. The attained results are outlined in Table 2 and presented in Figure 8. The results revealed that the MnCO₃ without ZrO_x yielded a 42% conversion of BzOH after 7 min, but after incorporating it with 1 wt.% of ZrO_x in MnCO₃, i.e., (1%)ZrO_x-MnCO₃, the effectiveness was noticeably enhanced and afforded a 74% conversion of alcohol under similar conditions (Table 2, entries 3 and 4). This was further increased to 100% conversion when 1% (w/w) of graphene oxide (GRO) was used as a catalyst support, i.e., (1%)ZrO_x-MnCO₃/(1%)GRO nanocomposite. This catalyst exhibited a significantly higher performance, yielding a complete BzOH conversion within an extremely short time of 7 min with a higher specific activity of 57.1 mmol/g·h (Table 2, entry 6). The enhanced catalytic performance of the catalyst using the GRO support could be due to the fact that GRO provides various oxygen-containing functional groups, which help achieve uniform and homogenous binding of ZrO_x-MnCO₃ onto the GRO. In return, the surface stabilization of the support (GRO) avoids the agglomeration of GRO sheets. This helps in increasing the surface area overall. In the present manuscript, the surface area of (1%)ZrO_x-MnCO₃/(1%)GRO (230 m²/g) was higher than the unsupported catalyst, i.e., (1%)ZrO_x-MnCO₃ (134 m²/g) and (1%)ZrO_x-MnCO₃/(1%)HRG (211 m²/g). These factors contributed to an enhancement of the overall catalytic efficacy upon inclusion of GRO.

Notably, upon comparing the results obtained with the catalytic performance of the HRG-incorporated catalyst system, i.e., (1%)ZrO_x-MnCO₃/(1%)HRG nanocomposite, reported earlier [52]. It was found that the (1%)ZrO_x-MnCO₃/(1%)HRG nanocomposite exhibited less catalytic activity. (1%)ZrO_x-MnCO₃/(1%)HRG yielded a 95.1% alcohol conversion with 54.3 mmol/g·h specific activity within 7 min at 100 °C, whereas (1%)ZrO_x-MnCO₃/(1%)GRO nanocomposite yielded 100% alcohol conversion with 57.1 mmol/g·h specific activity under identical conditions (Table 2, entry 5 and 6). The better performance of the catalyst using GRO support could be attributed to more homogenous growth of ZrO_x-MnCO₃ onto the support due to the presence of oxygenated functional groups, which also acts as a nucleation site. However, in case of HRG support, the nucleation sites are less in number, which results in more agglomerated growth of the active catalyst. We can conclude that the use of a GRO support for the preparation of metal oxide-based catalysts could be beneficial for homogeneous growth of the catalyst on the surface.

Table 2. Selective oxidation of BzOH catalyzed by various catalyst.

Entry	Catalyst	Surface Area (m ² /g)	Conversion (%)	Specific activity (mmol·g ⁻¹ ·h ⁻¹)	Selectivity (%)
1	HRG	78.2	2.0	1.2	>99
2	GRO	85.4	2.9	1.7	>99
3	MnCO ₃	70.5	42.6	24.3	>99
4	(1%)ZrO _x -MnCO ₃	133.6	74.4	42.5	>99
5	(1%)ZrO _x -MnCO ₃ /(1%)HRG	211.0	95.1	54.3	>99
6	(1%)ZrO _x -MnCO ₃ /(1%)GRO	229.5	100.0	57.1	>99

Conditions: 2 mmol of BzOH, 10 mL toluene, 0.3 g catalyst, 20 mL/min O₂ flow rate, 100 °C, 7 min.

2.2.3. Impact of Temperature

Commonly, the reaction temperature plays a fundamental role in the catalytic protocol and has an explicit effect on the efficiency and selectivity of a catalyst. Hence, the influence of temperature on BzOH oxidation was also estimated by varying the temperature from RT to 100 °C in the presence of the catalysts [MnCO₃, (1%)ZrO_x-MnCO₃, and (1%)ZrO_x-MnCO₃/(1%)GRO] by keeping the other parameters unchanged. The results obtained from the catalytic tests are depicted in Figure 9. The results displayed that the catalytic performance of all catalysts used in this study positively depend on the reaction temperatures.

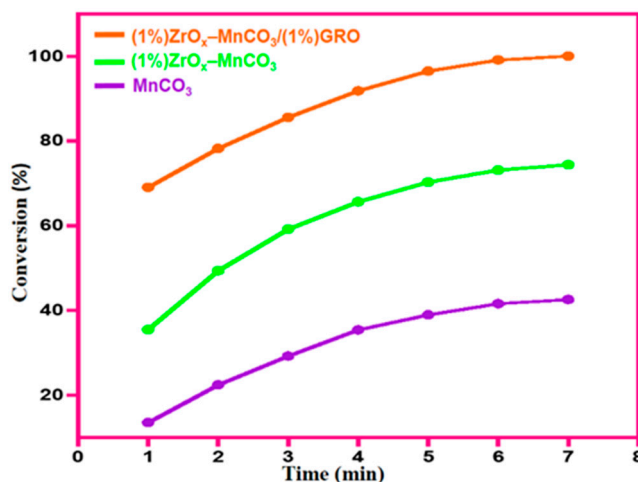


Figure 8. Influence of reaction time (min) on the catalytic activities of the as-prepared catalysts.

Meanwhile, a selectivity of >99% toward BzH was obtained for all catalysts. According to Figure 9, the best catalyst exhibited highest effectiveness is the (1%)ZrO_x-MnCO₃/(1%)GRO nanocomposite. At RT, a relatively low BzOH conversion of 38.2% was detected. As anticipated, a higher temperature contributed to a higher performance and led to a marked enhancement in the efficiency of the catalyst. At elevated temperatures (100 °C), a full alcohol conversion was achieved under identical conditions. The optimum performance within the conditions assessed was accomplished with a temperature of 100 °C. So, it was selected for further optimization studies.

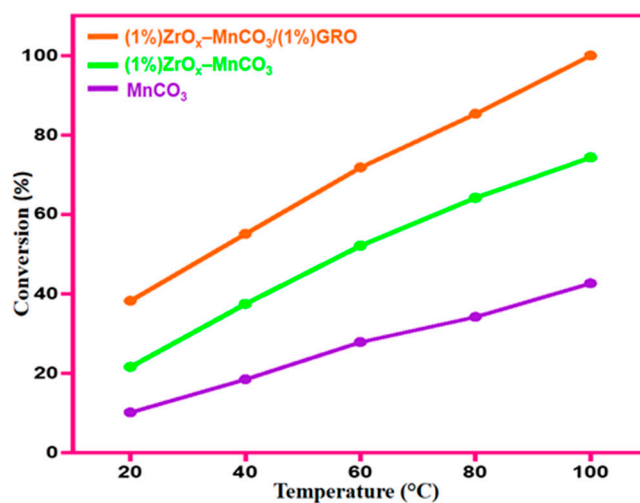


Figure 9. Impact of temperature on the oxidation of BzOH using the as-prepared catalysts.

2.2.4. Influence of Catalyst Quantity

The effect of the catalyst concentration on the selective oxidation of BzOH was examined by taking different amounts of catalysts (MnCO_3 , $(1\%)\text{ZrO}_x\text{-MnCO}_3$, and $(1\%)\text{ZrO}_x\text{-MnCO}_3/(1\%)\text{GRO}$), while keeping the other factors unchanged. The obtained results are presented in Figure 10. The data obtained distinctly illustrates that the alcohol conversion increased linearly as the quantity of catalysts increased from 0.05 to 0.3 g. Whereas, the BzH selectivity was almost constant during all oxidation reactions (>99%). For $(1\%)\text{ZrO}_x\text{-MnCO}_3/(1\%)\text{GRO}$ nanocomposite, when the catalyst concentration increased from 0.05 to 0.3 g, the conversion markedly raised from 28.07% to 100% after only 7 min at 100 °C. This study illustrated that only 0.3 g of the catalyst was required for achieving full transformation of BzOH within a relatively short period. Hence, it could be deduced that the performances of the as-fabricated catalysts were linearly proportional to the catalyst quantity as demonstrated in Figure 10.

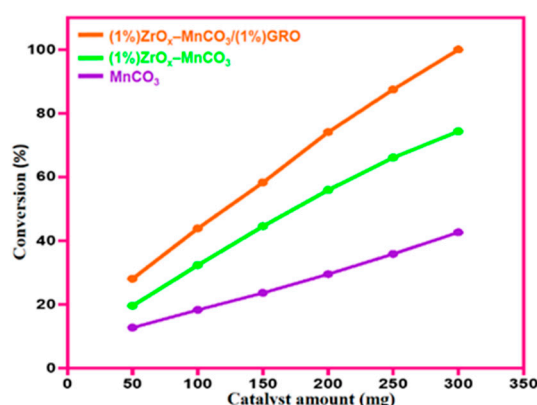


Figure 10. Impact of the quantity of the as-prepared catalysts on the catalytic properties.

Under the optimal circumstances, a blank reaction was conducted over the $(1\%)\text{ZrO}_x\text{-MnCO}_3/(1\%)\text{GRO}$ nanocomposite in the presence of the solvent, i.e., toluene, without reactant, i.e., BzOH, to ascertain that there is no role of the solvent in the oxidation of BzOH. It was found that no BzH was detected, indicating that the as-obtained BzH was from the catalytic oxidation of BzOH and not from toluene oxidation. Likewise, a blank experiment, i.e., the oxidation experiment conducted without the catalyst, at the optimized conditions was conducted to prove that the formed BzH was obtained due to the catalytic efficiency of the as-synthesized catalyst and not due to the self-oxidation of BzOH. It was observed that no BzH was formed, implying that the as-fabricated catalyst is indispensable for the current oxidation reaction. Moreover, to demonstrate the importance of the oxidant (O_2), the experiment was conducted in the presence of $(1\%)\text{ZrO}_x\text{-MnCO}_3/(1\%)\text{GRO}$ as catalyst using air without bubbling oxygen. Under the optimal circumstances, the results revealed the formation of 29.4% alcohol conversion, which is extremely lower than the 100% conversion obtained when the experiment was carried out with oxygen bubbling through the reaction mixture.

2.2.5. Catalyst Recovery

The catalyst recyclability is an essential aspect in the development of heterogeneous catalyst from both the scientific and industrial points of view. Reusability tests for $(1\%)\text{ZrO}_x\text{-MnCO}_3/(1\%)\text{GRO}$ nanocomposite were conducted by recovering the catalyst using centrifugation. The collected solid catalyst was washed thoroughly using toluene and then dried at 100 °C for 4 h to activate the catalyst. The dried catalyst was utilized for a consequent run under the conditions optimized earlier. The recycling results are demonstrated in Figure 11. The results demonstrate that the synthesized catalyst could be recycled 10 times without any obvious change of its performance after each recycling run. The conversion of BzOH was reduced slightly from 100% to 85% after 10 consecutive runs, maybe due to the inevitable loss of catalyst during the retrieving step [53]. It is noteworthy to mention that selectivity towards BzH was almost unchanged (above 99%) during the recyclability of the catalysts.

These obtained data indicate that the as-prepared catalysts are resistant to deactivation in the selective oxidation of BzOH. In order to overrule the mass-transport limitations of catalytic reactions during the recyclability study, this study was repeated under reaction conditions designed to yield a product less than 50%, which revealed an almost similar trend for the conversion of benzyl alcohol after three consecutive cycles. The data is provided in the Supplementary Material as Figure S3. We believe that in the present study, the mass transport limitations did not impact the catalytic efficiency. This could be because we did not use mesoporous materials nor thin films, where the substrate and product need to diffuse in and out. Here, in this study, the reaction took place at the surface of nanomaterials, which minimizes the effect of mass-transfer on the rate of reaction.

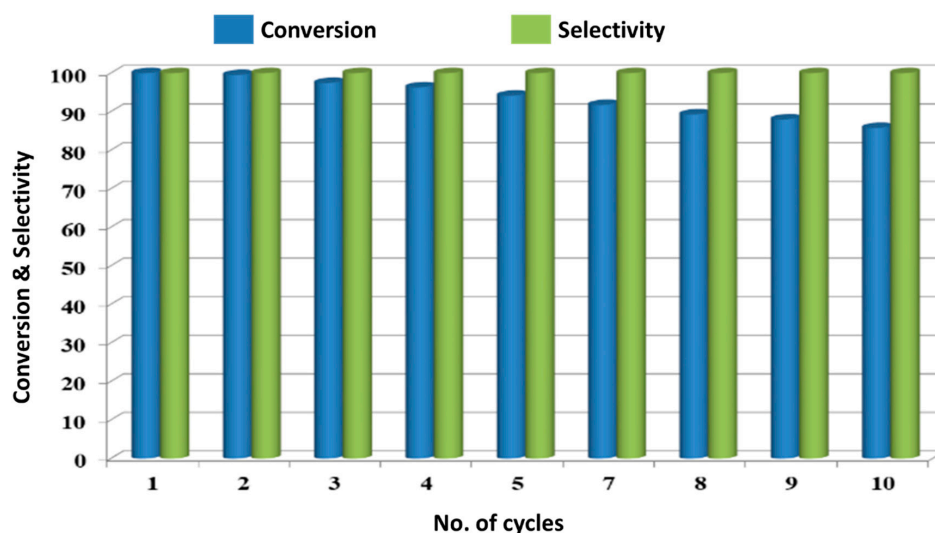


Figure 11. Reusability results of (1%)ZrO_x-MnCO₃/(1%)GRO nanocomposite. Conditions: 2 mmol BzOH, 0.3 g catalyst amount, 20 mL/min O₂ flow rate, 100 °C; 7 min.

Furthermore, to further show the remarkable catalytic efficiency of the (1%)ZrO_x-MnCO₃/(1%)GRO nanocomposite, this catalytic protocol was compared with other previously reported graphene-based catalysts as presented in Table 3. The results revealed that, among all the listed graphene-based catalysts, the (1%)ZrO_x-MnCO₃/(1%)GRO is the most efficient catalyst for BzOH oxidation in terms of conversion, reaction period, and specific activity. The (1%)ZrO_x-MnCO₃/(1%)GRO nanocomposite exhibited full conversion of BzOH and <99% BzH selectivity after a short time (7 min) with perfect specific activity (57.1 mmol/g·h). As displayed in Table 3, other graphene-based catalysts exhibited a relatively longer time for a full transformation of BzOH and the (1%)ZrO_x-MnCO₃/(1%)GRO nanocomposite had the highest specific activity (57.1 mmol/g·h).

Table 3. Catalytic activity comparisons of different graphene catalysts for the catalytic oxidation of BzOH to BzH.

Catalyst	Conversion (%)	Selectivity (%)	T. (°C)	Time (h)	Specific Activity (mmol/g·h)	Ref.
(1%)ZrO _x -MnCO ₃ /(1%)GRO	100	>99	100	0.12	57.1	Herein
(1%)ZrO _x -MnCO ₃ /(1%)HRG	95.1	>99	100	0.12	54.3	[52]
0.3Sn-W/RGO	94	94.3	80	3	15.7	[50]
Cu@rGO	>99	98.6	80	16	8.3	[54]
MnO ₂ /GO (10/100)	97	100	110	3	1.6	[51]
abGO	93.1	100	100	30	0.16	[55]
Pd NPs/GO	36	34.1	110	6	1.0	[56]
Cu(II)@AFGO	92	99	70	3	2.0	[57]
GO-100	100	100	80	5	1.1	[58]
GO/Fe ₃ O ₄ /HPW	99	100	70	3	16.7	[41]
Au NPs/RGO	65	93	100	8	5.4	[53]
(NH ₄) ₅ H ₅ [H ₂ (WO ₄) ₆]/GO	91	–	70	11	2.8	[59]
Ag ₂ O-MnO ₂ /HRG	100	>99	100	0.6	11.4	[60]
NGO	96	–	80	12	3.8	[61]
Ag NPs/GO	33	55	80	24	2.8	[62]
Ti(SO ₄) ₂ /GOF	91.5	98.8	Reflux	4	38.09	[63]
GO-N-PW	76	99	100	6	10.6	[64]

2.2.6. General Applicability

In order to demonstrate the generality of the (1%)ZrO_x-MnCO₃/(1%)GRO catalyst, several aromatic, aliphatic, allylic, heterocyclic, primary, and secondary alcohols were subjected to oxidation using O₂ as an environmentally benign oxidant under optimal conditions (Table 4, entries 1–37). The obtained data are summarized in Table 4. To our delight, all aromatic alcohols were transformed smoothly to their corresponding aldehydes in full conversions after short times without any detectable further oxidation to carboxylic acids (Table 4, entries 1–22). The oxidation of the aromatic alcohols was significantly influenced by the electronic properties of the groups on the phenyl group. Usually, the benzylic alcohols, which were substituted with electron-releasing groups, exhibited higher activity than the alcohols carrying electron-withdrawing groups [54]. The higher catalytic efficiency in the case of alcohols possessing electron-releasing substituents could be due to the sufficient electron density in the active center by comparing the substrates containing electron-withdrawing substituents. For instance, oxidation of aromatic alcohol-carrying electron-releasing substituents, like 4-methoxybenzyl alcohol, yielded full conversion after 7 min (Table 4, entry 2), while oxidation of alcohol containing an electron-withdrawing substituent, like 4-nitrobenzyl alcohol, gave 100% conversion after a relatively longer time (13 min) (Table 4, entry 15). Besides, it was found that para-substituted benzyl alcohols possess higher activities compared to ortho- and meta-positions. That might be due to the para-derivative having the lowest steric hindrance by compared with the other positions [49], such as para-nitrobenzyl alcohol, was fully oxidized to para-nitrobenzaldehyde within just 13 min, while meta- and ortho-nitrobenzyl alcohol were fully converted after a longer time of 15 and 18 min, respectively (Table 4, entries 17 and 19). In addition, steric resistance is also another fundamental factor that affects the oxidation rate. The bulky substituents (e.g., 2,3,4-Trimethoxy, 2,4-Dichloro, and 2,3,4,5,6-Pentafluoro) connected to the aromatic alcohol reduces the oxidation rate and required a longer period, which could be due to the steric hinderance that hinders the oxidation of bulky alcohols (Table 4, entries 16,18,20) [65]. Regarding allylic alcohols, cinnamyl alcohol was selectively oxidized to cinnamaldehyde in a relatively short period of 12 min (Table 4, entry 23). Furthermore, a furfuryl alcohol as an example of heterocyclic alcohols was fully converted to furfural within 22 min with >99% furfural selectivity (Table 4, entry 24).

Almost, all aromatic secondary alcohols were selectively converted to their respective ketones with entire conversion under similar circumstances (Table 4, entries 25–30). As an example, diphenylmethanol was transformed into its respective ketone with 100% conversion within only 8 min, whereas 4-chloro-diphenylmethanol yielded 100% conversion after a relatively longer time of 10 min. This was probably due to 4-chloro-diphenylmethanol carrying an electron-withdrawing substituent that deactivates the aromatic ring by reducing the electron density (Table 4, entries 26 and 27).

The oxidation of aromatic alcohols occurs more readily than for their aliphatic counterparts [50]. In fact, the present catalytic strategy was also found to be a highly effective catalyst for the oxidation of primary aliphatic alcohols into their respective aldehydes. In this context, a full transformation of cyclohexanemethanol and 5-Hexen-1-ol to their corresponding aldehydes was accomplished by prolonging the reaction time (Table 4, entries 31 and 32). Likewise, compared to secondary aromatic alcohols, the oxidation of secondary aliphatic alcohols afforded relatively low activity towards the oxidation process (Table 4, entries 35–37). As anticipated, it was necessary to prolong the reaction time because the oxidation of aromatic secondary alcohols is much easier than the oxidation of aliphatic secondary alcohols, like 2-octanol (Table 4, entry 37). As a consequence, it can be stated that the selective oxidation of alcohols using (1%)ZrO_x-MnCO₃/(1%)GRO catalyst was influenced by two parameters, electronic and steric effects. The NMR spectrum of a few aldehydes is given in Figure S4–S8.

Table 4. Catalytic oxidation of various kinds alcohols over (1%)ZrO_x-MnCO₃/(1%)GRO.

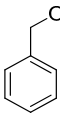
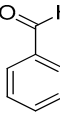
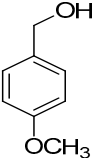
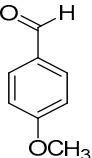
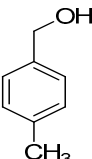
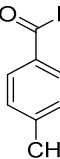
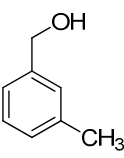
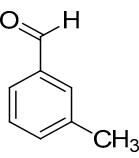
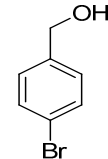
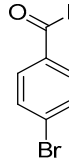
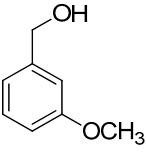
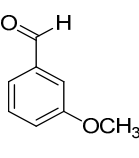
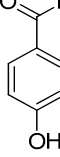
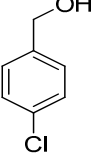
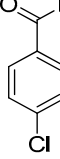
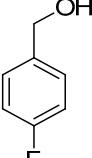
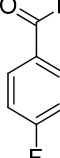
Entry	Reactant	Product	Time (min)	Conversion (%)	Selectivity (%)
1			7	100	>99
2			7	100	>99
3			8	100	>99
4			8	100	>99
5			9	100	>99
6			9	100	>99
7			10	100	>99
8			10	100	>99
9			11	100	>99

Table 4. Cont.

Entry	Reactant	Product	Time (min)	Conversion (%)	Selectivity (%)
10			12	100	>99
11			12	100	>99
12			12	100	>99
13			13	100	>99
14			14	100	>99
15			13	100	>99
16			12	100	>99
17			15	100	>99
18			19	100	>99

Table 4. Cont.

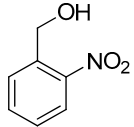
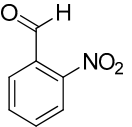
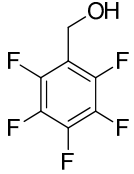
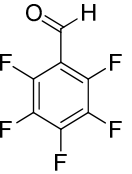
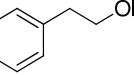
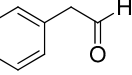
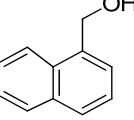
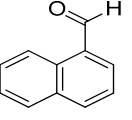
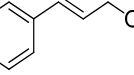
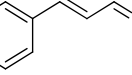
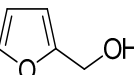
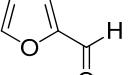
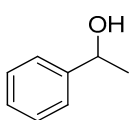
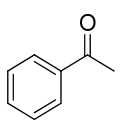
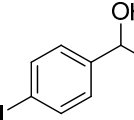
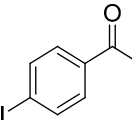
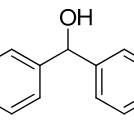
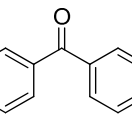
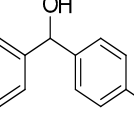
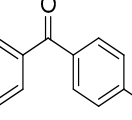
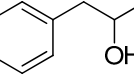
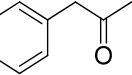
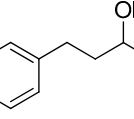
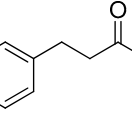
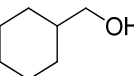
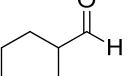
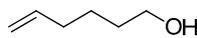
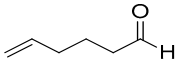
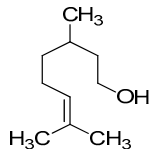
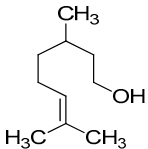
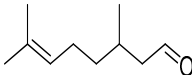
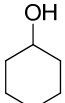
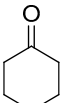
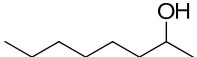
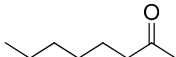
Entry	Reactant	Product	Time (min)	Conversion (%)	Selectivity (%)
19			18	100	>99
20			22	100	>99
21			15	100	>99
22			24	100	>99
23			12	100	>99
24			22	100	>99
25			6	100	>99
26			8	100	>99
27			8	100	>99
28			12	100	>99
29			12	100	>99
30			15	100	>99
31			25	100	>99

Table 4. Cont.

Entry	Reactant	Product	Time (min)	Conversion (%)	Selectivity (%)
32			95	100	>99
33			100	100	>99
34			110	100	>99
35			30	100	>99
36			90	100	>99
37			100	100	>99

Conditions: 2 mmol of substrate, 0.3 g (1%)ZrO_x-MnCO₃/GRO catalyst, 20 mL/min O₂ flow rate, 100 °C.

3. Materials and Methods

3.1. Preparation of GRO

Firstly, GRO was synthesized from pristine graphite using the Hummers procedure [66].

3.2. Preparation of (1%)ZrO_x-MnCO₃/GRO Nanocomposite

The ZrO_x-doped MnCO₃ was synthesized using the co-precipitation method. Briefly, stoichiometric amounts of Mn(NO₃)₂ and Zr(NO₃)₂ were dissolved in distilled water (100 mL) followed by the addition of a solution of sodium hydrogen carbonate (0.5 M) at 100 °C, until the pH of the solution reached 9, then the solution was left to stir for 3 hours. The stirring was continued overnight at room temperature (RT). The reaction mixture was filtered using centrifugation and dried at 70 °C overnight. The obtained product was calcined in a muffle furnace at 300 °C. Then, the previously synthesized GRO dried at 70 °C was incorporated in the ZrO_x-doped MnCO₃ by milling in order to obtain the desired (1%)ZrO_x-MnCO₃/GRO nanocomposite. It is worth mentioning that if GRO was introduced prior to calcination, there was a loss of weight and catalytic efficiency.

3.3. Characterization

The as-fabricated nanocomposites were analyzed using different spectroscopic, microscopic, and X-ray-based characterization instruments.

3.4. Catalytic Tests

The experimental method used for the alcohol oxidation is described in our previously reported paper [52] Briefly, a solution of benzyl alcohol in toluene and catalyst was heated to reflux temperature and oxygen was bubbled through the solution. Periodically, the reaction mixture was collected and subjected to GC analysis and the conversion was monitored.

4. Conclusions

Here, we presented an efficient, robust, cost effective, and recoverable catalytic system for selective alcohol oxidation with 100% convertibility and selectivity. We compared (1%)ZrO_x-MnCO₃, (1%)ZrO_x-MnCO₃/(1%)HRG and (1%)ZrO_x-MnCO₃/(1%)GRO for BzOH oxidation using O₂ as an environmentally benign oxidant under alkali-free conditions. (1%)ZrO_x-MnCO₃/(1%)GRO yielded a higher performance (100% conversion) than the (1%)ZrO_x-MnCO₃ and (1%)ZrO_x-MnCO₃/(1%)HRG catalysts. In addition, we found that post-calcination addition of GRO resulted in better catalytic efficacy. This superior activity of (1%)ZrO_x-MnCO₃/(1%)GRO could be due to the high surface area, perfect chemical stability and compatibility, efficient mechanical and thermal stability, and the existence of myriad oxygenic functionalities on GRO sheets. The physical mixing at room temperature avoided the thermal degradation of oxygenated functional groups. (1%)ZrO_x-MnCO₃/(1%)GRO exhibited a complete BzOH conversion with >99% BzH selectivity within an extremely short time at comparatively low temperatures, i.e., 100 °C. The achieved specific activity (57.1 mmol/g·h) was much higher (at 100 °C) than that presented in previously reported studies. Moreover, various types of alcohols were assessed for oxidation to their respective carbonyls with much better yields. Our catalytic methodology was quite selective, producing only required aldehydes or ketones without further oxidation to acids. The highlights of the present catalytic protocol are as follows: (a) Simple and straightforward synthetic method, (b) cheap and environment-friendly oxidant; (c) no use of any additives or alkalis, (d) cost-effective catalyst, (e) mild conditions, (f) full convertibility and selectivity, (g) rapid process, (h) recoverable catalyst, and (i) applicable to a variety of alcohols. All these merits will cause this catalytic system to be very useful and have wide application prospects in other organic synthetic transformations.

Supplementary Materials: The following are available online at <http://www.mdpi.com/2073-4344/9/9/759/s1>.

Author Contributions: S.F.A. and M.N.T. designed the project; M.E.A., M.K. (Mujeeb Khen), and M.R.S. helped to draft the manuscript; M.E.A. and M.K. (Mufsir Kuniyil) carried out the experimental part and some part of characterization; N.M.A. and M.S. carried out the some part of characterization; M.M.A. carried out the SEM analysis. J.A.M. contributed towards studies required for revision of the manuscript. A.A.-W. and M.R.H.S. provided scientific guidance for successful completion of the project and helped to draft the manuscript. All authors read and approved the final manuscript.

Funding: This work was funded by Deanship of Scientific Research at King Saud University for funding this work through the research group project No. RG-1436-032.

Acknowledgments: The authors extend their appreciation to the Deanship of Scientific Research at King Saud University for funding this work through the research group project No. RG-1436-032.

Conflicts of Interest: The authors declare no conflict of interest.

References

1. Arena, F.; Gumina, B.; Cannilla, C.; Spadaro, L.; Patti, A.; Spiccia, L. Nanostructured MnO_x catalysts in the liquid phase selective oxidation of benzyl alcohol with oxygen: Part II. Reaction mechanism, kinetics and deactivation pattern. *Appl. Catal. B Environ.* **2015**, *170*, 233–240. [CrossRef]
2. Zhan, G.; Hong, Y.; Mbah, V.T.; Huang, J.; Ibrahim, A.-R.; Du, M.; Li, Q. Bimetallic Au-Pd/MgO as Efficient Catalysts for Aerobic Oxidation of Benzyl Alcohol: A Green Bio-Reducing Preparation Method. *Appl. Catal. A* **2012**, *439*, 179–186. [CrossRef]
3. Chen, G.; Wu, S.; Liu, H.; Jiang, H.; Li, Y. Palladium supported on an acidic metal-organic framework as an efficient catalyst in selective aerobic oxidation of alcohols. *Green Chem.* **2013**, *15*, 230–235. [CrossRef]
4. Arena, F.; Gumina, B.; Lombardo, A.F.; Espro, C.; Patti, A.; Spadaro, L.; Spiccia, L. Nanostructured MnO_x Catalysts in the Liquid Phase Selective Oxidation of Benzyl Alcohol with Oxygen: Part I. Effects of Ce and Fe Addition on Structure and Reactivity. *Appl. Catal. B Environ.* **2015**, *162*, 260–267. [CrossRef]

5. Parmeggiani, C.; Cardona, F. Transition Metal Based Catalysts in the Aerobic Oxidation of Alcohols. *Green Chem.* **2012**, *14*, 547–564. [[CrossRef](#)]
6. Wang, T.; Yuan, X.; Li, S.; Zeng, L.; Gong, J. CeO₂-modified Au@SBA-15 nanocatalysts for liquid-phase selective oxidation of benzyl alcohol. *Nanoscale* **2015**, *7*, 7593–7602. [[CrossRef](#)] [[PubMed](#)]
7. Zhou, C.; Guo, Z.; Dai, Y.; Jia, X.; Yu, H.; Yang, Y. Promoting role of bismuth on carbon nanotube supported platinum catalysts in aqueous phase aerobic oxidation of benzyl alcohol. *Appl. Catal. B Environ.* **2016**, *181*, 118–126. [[CrossRef](#)]
8. Zhang, L.; Zhou, N.; Wang, B.; Liu, C.; Zhu, G. Fabrication of Fe₃O₄/PAH/PSS@Pd core-shell microspheres by layer-by-layer assembly and application in catalysis. *J. Colloid Interface Sci.* **2014**, *421*, 1–5. [[CrossRef](#)]
9. Ji, H.-B.; Yuan, Q.-L.; Zhou, X.-T.; Pei, L.-X.; Wang, L.-F. Highly efficient selective oxidation of alcohols to carbonyl compounds catalyzed by ruthenium (III) meso-tetraphenylporphyrin chloride in the presence of molecular oxygen. *Bioorg. Med. Chem. Lett.* **2007**, *17*, 6364–6368. [[CrossRef](#)]
10. Xie, M.; Dai, X.; Meng, S.; Fu, X.; Chen, S. Selective oxidation of aromatic alcohols to corresponding aromatic aldehydes using In₂S₃ microsphere catalyst under visible light irradiation. *Chem. Eng. J.* **2014**, *245*, 107–116. [[CrossRef](#)]
11. Bai, C.; Li, A.; Yao, X.; Liu, H.; Li, Y. Efficient and selective aerobic oxidation of alcohols catalysed by MOF-derived Co catalysts. *Green Chem.* **2016**, *18*, 1061–1069. [[CrossRef](#)]
12. Song, H.; Kang, B.; Hong, S.H. Fe-catalyzed acceptorless dehydrogenation of secondary benzylic alcohols. *ACS Catal.* **2014**, *4*, 2889–2895. [[CrossRef](#)]
13. Lin, L.; Juanjuan, M.; Liuyan, J.; Yunyang, W. Molecular sieve promoted copper catalyzed aerobic oxidation of alcohols to corresponding aldehydes or ketones. *J. Mol. Catal. A Chem.* **2008**, *291*, 1–4. [[CrossRef](#)]
14. Biradar, A.V.; Dongare, M.K.; Umbarkar, S.B. Selective oxidation of aromatic primary alcohols to aldehydes using molybdenum acetylido-oxo-peroxo complex as catalyst. *Tetrahedron Lett.* **2009**, *50*, 2885–2888. [[CrossRef](#)]
15. Jiang, N.; Ragauskas, A.J. Vanadium-catalyzed selective aerobic alcohol oxidation in ionic liquid [bmim]PF₆. *Tetrahedron Lett.* **2007**, *48*, 273–276. [[CrossRef](#)]
16. Forouzani, M.; Mardani, H.R.; Ziari, M.; Malekzadeh, A.; Biparva, P. Comparative Study of Oxidation of Benzyl Alcohol: Influence of Cu-Doped Metal Cation on Nano ZnO Catalytic Activity. *Chem. Eng. J.* **2015**, *275*, 220–226. [[CrossRef](#)]
17. Adil, S.F.; Alabbad, S.; Kuniyil, M.; Khan, M.; Alwarthan, A.; Mohri, N.; Tremel, W.; Tahir, M.N.; Siddiqui, M.R. Vanadia supported on nickel manganese oxide nanocatalysts for the catalytic oxidation of aromatic alcohols. *Nanoscale Res. Lett.* **2015**, *10*, 52. [[CrossRef](#)] [[PubMed](#)]
18. Pokharel, P.; Truong, Q.-T. Multi-step microwave reduction of graphite oxide and its use in the formation of electrically conductive graphene/epoxy composites. *Compos. Part B Eng.* **2014**, *64*, 187–193. [[CrossRef](#)]
19. Shinde, V.M.; Skupien, E.; Makkee, M. Synthesis of Highly Dispersed Pd Nanoparticles Supported on Multi-Walled Carbon Nanotubes and Their Excellent Catalytic Performance for Oxidation of Benzyl Alcohol. *Catal. Sci. Technol.* **2015**, *5*, 4144–4153. [[CrossRef](#)]
20. Zhu, S.; Wang, J.; Fan, W. Graphene-based catalysis for biomass conversion. *Catal. Sci. Technol.* **2015**, *5*, 3845–3858. [[CrossRef](#)]
21. Navalon, S.; Dhakshinamoorthy, A.; Alvaro, M.; Garcia, H. Carbocatalysis by graphene-based materials. *Chem. Rev.* **2014**, *114*, 6179–6212. [[CrossRef](#)] [[PubMed](#)]
22. Nie, R.; Wang, J.; Wang, L.; Qin, Y.; Chen, P.; Hou, Z. Platinum Supported on Reduced Graphene Oxide as a Catalyst for Hydrogenation of Nitroarenes. *Carbon* **2012**, *50*, 586–596. [[CrossRef](#)]
23. Primo, A.; Puche, M.; Pavel, O.D.; Cojocaru, B.; Tirsoaga, A.; Parvulescu, V.; García, H. Graphene oxide as a metal-free catalyst for oxidation of primary amines to nitriles by hypochlorite. *Chem. Commun.* **2016**, *52*, 1839–1842. [[CrossRef](#)] [[PubMed](#)]
24. Shao, L.; Huang, X.; Teschner, D.; Zhang, W. Gold supported on graphene oxide: An active and selective catalyst for phenylacetylene hydrogenations at low temperatures. *ACS Catal.* **2014**, *4*, 2369–2373. [[CrossRef](#)]
25. Sun, W.; Lu, X.; Tong, Y.; Zhang, Z.; Lei, J.; Nie, G.; Wang, C. Fabrication of highly dispersed palladium/graphene oxide nanocomposites and their catalytic properties for efficient hydrogenation of p-nitrophenol and hydrogen generation. *Int. J. Hydrogen Energy* **2014**, *39*, 9080–9086. [[CrossRef](#)]

26. Liu, Y.; Jin, W.; Zhao, Y.; Zhang, G.; Zhang, W. Enhanced catalytic degradation of methylene blue by α -Fe₂O₃/graphene oxide via heterogeneous photo-Fenton reactions. *Appl. Catal. B Environ.* **2017**, *206*, 642–652. [[CrossRef](#)]
27. Xu, C.; Wang, X.; Zhu, J.; Yang, X.; Lu, L. Deposition of Co₃O₄ nanoparticles onto exfoliated graphite oxide sheets. *J. Mater. Chem.* **2008**, *18*, 5625–5629. [[CrossRef](#)]
28. Jafari, A.J.; Kalantary, R.R.; Esrafil, A.; Arfaenia, H. Synthesis of silica-functionalized graphene oxide/ZnO coated on fiberglass and its application in photocatalytic removal of gaseous benzene. *Process Saf. Environ. Prot.* **2018**, *116*, 377–387. [[CrossRef](#)]
29. Mahyari, M.; Shaabani, A. Graphene Oxide-Iron Phthalocyanine Catalyzed Aerobic Oxidation of Alcohols. *Appl. Catal. A* **2014**, *469*, 524–531. [[CrossRef](#)]
30. Arumugam, S.; Mohan, B.C.; Vasudevan, S.V.; Vanaraj, R.; Rukmanikrishnan, B.; Periyasamy, T.; Asrafali, S.P. Selective Oxidation of Cyclohexane Using Graphene Oxide-Supported Ceria Nanocomposites with Exposed Active {1 0 0} Facets. *ChemistrySelect* **2017**, *2*, 6223–6230. [[CrossRef](#)]
31. Rana, S.; Jonnalagadda, S.B. CuO/Graphene Oxide Nanocomposite as Highly Active and Durable Catalyst for Selective Oxidation of Cyclohexane. *ChemistrySelect* **2017**, *2*, 2277–2281. [[CrossRef](#)]
32. Su, C.; Acik, M.; Takai, K.; Lu, J.; Hao, S.-j.; Zheng, Y.; Wu, P.; Bao, Q.; Enoki, T.; Chabal, Y.J. Probing the catalytic activity of porous graphene oxide and the origin of this behaviour. *Nat. Commun.* **2012**, *3*, 1298. [[CrossRef](#)] [[PubMed](#)]
33. Zhao, Q.; Bai, C.; Zhang, W.; Li, Y.; Zhang, G.; Zhang, F.; Fan, X. Catalytic epoxidation of olefins with graphene oxide supported copper (Salen) complex. *Ind. Eng. Chem. Res.* **2014**, *53*, 4232–4238. [[CrossRef](#)]
34. Wang, C.; Hu, L.; Hu, Y.; Ren, Y.; Chen, X.; Yue, B.; He, H. Direct hydroxylation of benzene to phenol over metal oxide supported graphene oxide catalysts. *Catal. Commun.* **2015**, *68*, 1–5. [[CrossRef](#)]
35. Diao, J.; Liu, H.; Wang, J.; Feng, Z.; Chen, T.; Miao, C.; Yang, W.; Su, D.S. Porous graphene-based material as an efficient metal free catalyst for the oxidative dehydrogenation of ethylbenzene to styrene. *Chem. Commun.* **2015**, *51*, 3423–3425. [[CrossRef](#)]
36. Sandhya, P.; Jose, J.; Sreekala, M.; Padmanabhan, M.; Kalarikkal, N.; Thomas, S. Reduced graphene oxide and ZnO decorated graphene for biomedical applications. *Ceram. Int.* **2018**, *44*, 15092–15098. [[CrossRef](#)]
37. Xie, G.; Xi, P.; Liu, H.; Chen, F.; Huang, L.; Shi, Y.; Hou, F.; Zeng, Z.; Shao, C.; Wang, J. A facile chemical method to produce superparamagnetic graphene oxide–Fe₃O₄ hybrid composite and its application in the removal of dyes from aqueous solution. *J. Mater. Chem.* **2012**, *22*, 1033–1039. [[CrossRef](#)]
38. Zhang, S.; Zhu, L.; Song, H.; Chen, X.; Wu, B.; Zhou, J.; Wang, F. How graphene is exfoliated from graphitic materials: Synergistic effect of oxidation and intercalation processes in open, semi-closed, and closed carbon systems. *J. Mater. Chem.* **2012**, *22*, 22150–22154. [[CrossRef](#)]
39. Assal, M.E.; Kuniyil, M.; Khan, M.; Al-Warthan, A.; Siddiqui, M.R.H.; Tremel, W.; Nawaz Tahir, M.; Adil, S.F. Synthesis and comparative catalytic study of zirconia–MnCO₃ or–Mn₂O₃ for the oxidation of benzylic alcohols. *ChemOpen* **2017**, *6*, 112–120.
40. Sharma, P.; Darabdhara, G.; Reddy, T.M.; Borah, A.; Bezboruah, P.; Gogoi, P.; Hussain, N.; Sengupta, P.; Das, M.R. Synthesis, characterization and catalytic application of Au NPs-reduced graphene oxide composites material: An eco-friendly approach. *Catal. Commun.* **2013**, *40*, 139–144. [[CrossRef](#)]
41. Darvishi, K.; Amani, K.; Rezaei, M. Preparation, characterization and heterogeneous catalytic applications of GO/Fe₃O₄/HPW nanocomposite in chemoselective and green oxidation of alcohols with aqueous H₂O₂. *Appl. Organomet. Chem.* **2018**, *32*, e4323. [[CrossRef](#)]
42. Metin, Ö.; Kayhan, E.; Özkar, S.; Schneider, J.J. Palladium Nanoparticles Supported on Chemically Derived Graphene: An Efficient and Reusable Catalyst for the Dehydrogenation of Ammonia Borane. *Int. J. Hydrogen Energy* **2012**, *37*, 8161–8169. [[CrossRef](#)]
43. Kang, J.H.; Kim, T.; Choi, J.; Park, J.; Kim, Y.S.; Chang, M.S.; Jung, H.; Park, K.T.; Yang, S.J.; Park, C.R. Hidden second oxidation step of Hummers method. *Chem. Mater.* **2016**, *28*, 756–764. [[CrossRef](#)]
44. Qiu, T.; Wang, J.; Lu, Y.; Yang, W. Facile Fabrication of Chinese Lantern-Like MnO@N-C: A High-Performance Anode Material for Lithium-Ion Batteries. *RSC Adv.* **2014**, *4*, 23027–23035. [[CrossRef](#)]
45. Atchudan, R.; Edison, T.N.J.I.; Perumal, S.; Karthikeyan, D.; Lee, Y.R. Facile synthesis of zinc oxide nanoparticles decorated graphene oxide composite via simple solvothermal route and their photocatalytic activity on methylene blue degradation. *J. Photochem. Photobiol. B* **2016**, *162*, 500–510. [[CrossRef](#)] [[PubMed](#)]

46. Gurunathan, S.; Han, J.W.; Eppakayala, V.; Kim, J.-H. Microbial reduction of graphene oxide by *Escherichia coli*: A green chemistry approach. *Colloids Surf. B* **2013**, *102*, 772–777. [[CrossRef](#)] [[PubMed](#)]
47. Huang, H.; Yue, Z.; Li, G.; Wang, X.; Huang, J.; Du, Y.; Yang, P. Ultraviolet-assisted preparation of mesoporous WO₃/reduced graphene oxide composites: Superior interfacial contacts and enhanced photocatalysis. *J. Mater. Chem. A* **2013**, *1*, 15110–15116. [[CrossRef](#)]
48. Li, Y.; Lv, X.; Lu, J.; Li, J. Preparation of SnO₂-nanocrystal/graphene-nanosheets composites and their lithium storage ability. *J. Phys. Chem. C* **2010**, *114*, 21770–21774. [[CrossRef](#)]
49. Kadam, M.M.; Dhopte, K.B.; Jha, N.; Gaikar, V.G.; Nemade, P.R. Synthesis, characterization and application of γ -MnO₂/graphene oxide for the selective aerobic oxidation of benzyl alcohols to corresponding carbonyl compounds. *New J. Chem.* **2016**, *40*, 1436–1442. [[CrossRef](#)]
50. Xu, C.; Zhang, L.; An, Y.; Wang, X.; Xu, G.; Chen, Y.; Dai, L. Promotional synergistic effect of Sn doping into a novel bimetallic Sn-W oxides/graphene catalyst for selective oxidation of alcohols using aqueous H₂O₂ without additives. *Appl. Catal. A* **2018**, *558*, 26–33. [[CrossRef](#)]
51. Hu, Z.; Zhao, Y.; Liu, J.; Wang, J.; Zhang, B.; Xiang, X. Ultrafine MnO₂ nanoparticles decorated on graphene oxide as a highly efficient and recyclable catalyst for aerobic oxidation of benzyl alcohol. *J. Colloid Interface Sci.* **2016**, *483*, 26–33. [[CrossRef](#)] [[PubMed](#)]
52. Assal, M.E.; Shaik, M.R.; Kuniyil, M.; Khan, M.; Al-Warthan, A.; Siddiqui, M.R.H.; Khan, S.M.; Tremel, W.; Tahir, M.N.; Adil, S.F. A highly reduced graphene oxide/ZrO_x-MnCO₃ or-Mn₂O₃ nanocomposite as an efficient catalyst for selective aerial oxidation of benzylic alcohols. *RSC Adv.* **2017**, *7*, 55336–55349. [[CrossRef](#)]
53. Yu, X.; Huo, Y.; Yang, J.; Chang, S.; Ma, Y.; Huang, W. Reduced Graphene Oxide Supported Au Nanoparticles as an Efficient Catalyst for Aerobic Oxidation of Benzyl Alcohol. *Appl. Surf. Sci.* **2013**, *280*, 450–455. [[CrossRef](#)]
54. Feng, X.; Lv, P.; Sun, W.; Han, X.; Gao, L.; Zheng, G. Reduced graphene oxide-supported Cu nanoparticles for the selective oxidation of benzyl alcohol to aldehyde with molecular oxygen. *Catal. Commun.* **2017**, *99*, 105–109. [[CrossRef](#)]
55. Zhu, S.; Cen, Y.; Yang, M.; Guo, J.; Chen, C.; Wang, J.; Fan, W. Probing the intrinsic active sites of modified graphene oxide for aerobic benzylic alcohol oxidation. *Appl. Catal. B Environ.* **2017**, *211*, 89–97. [[CrossRef](#)]
56. Wu, G.; Wang, X.; Guan, N.; Li, L. Palladium on graphene as efficient catalyst for solvent-free aerobic oxidation of aromatic alcohols: Role of graphene support. *Appl. Catal. B Environ.* **2013**, *136*, 177–185. [[CrossRef](#)]
57. Rana, S.; Jonnalagadda, S.B. Cu doped amine functionalized graphene oxide and its scope as catalyst for selective oxidation. *Catal. Commun.* **2017**, *100*, 183–186. [[CrossRef](#)]
58. Geng, L.; Wu, S.; Zou, Y.; Jia, M.; Zhang, W.; Yan, W.; Liu, G. Correlation between the Microstructures of Graphite Oxides and Their Catalytic Behaviors in Air Oxidation of Benzyl Alcohol. *J. Colloid Interface Sci.* **2014**, *421*, 71–77. [[CrossRef](#)]
59. Fu, H.; Hu, C.; Huang, Z.; Zhou, J.; Peng, X. Ammonium Tungstate as an Effective Catalyst for Selective Oxidation of Alcohols to Aldehydes or Ketones with Hydrogen Peroxide under Water—A Synergy of Graphene Oxide. *Synlett* **2018**, *29*, 447–451.
60. Assal, M.E.; Shaik, M.R.; Kuniyil, M.; Khan, M.; Al-Warthan, A.; Alharthi, A.I.; Varala, R.; Siddiqui, M.R.H.; Adil, S.F. Ag₂O nanoparticles/MnCO₃,-MnO₂ or-Mn₂O₃/highly reduced graphene oxide composites as an efficient and recyclable oxidation catalyst. *Arab. J. Chem.* **2019**, *12*, 54–68. [[CrossRef](#)]
61. Sedrpoushan, A.; Heidari, M.; Akhavan, O. Nanoscale graphene oxide sheets as highly efficient carbocatalysts in green oxidation of benzylic alcohols and aromatic aldehydes. *Chin. J. Catal.* **2017**, *38*, 745–757. [[CrossRef](#)]
62. Zahed, B.; Hosseini-Monfared, H. A Comparative Study of Silver-Graphene Oxide Nanocomposites as a Recyclable Catalyst for the Aerobic Oxidation of Benzyl Alcohol: Support Effect. *Appl. Surf. Sci.* **2015**, *328*, 536–547. [[CrossRef](#)]
63. Ma, W.; Tong, Q.; Wang, J.; Yang, H.; Zhang, M.; Jiang, H.; Wang, Q.; Liu, Y.; Cheng, M. Synthesis and characterization of titanium (IV)/graphene oxide foam: A sustainable catalyst for the oxidation of benzyl alcohol to benzaldehyde. *RSC Adv.* **2017**, *7*, 6720–6723. [[CrossRef](#)]

64. Liu, K.; Chen, T.; Hou, Z.; Wang, Y.; Dai, L. Graphene Oxide as Support for the Immobilization of Phosphotungstic Acid: Application in the Selective Oxidation of Benzyl Alcohol. *Catal. Lett.* **2014**, *144*, 314–319. [[CrossRef](#)]
65. Borthakur, R.; Asthana, M.; Kumar, A.; Lal, R.A. Cooperative Catalysis by Polymetallic Copper–Zinc Complexes in the Efficient Oxidation of Alcohols under Solvent Free Condition. *Inorg. Chem. Commun.* **2014**, *46*, 198–201. [[CrossRef](#)]
66. William, S.; Hummers, J.; Offeman, R.E. Preparation of graphitic oxide. *J. Am. Chem. Soc.* **1958**, *80*, 1339.



© 2019 by the authors. Licensee MDPI, Basel, Switzerland. This article is an open access article distributed under the terms and conditions of the Creative Commons Attribution (CC BY) license (<http://creativecommons.org/licenses/by/4.0/>).